Global Pmag Seminar
Oct 15, 2013
Lisa Tauxe

- Fanjat et al. 2013, First archeointensity determinations on Maya incense burners from Palenque temples, Mexico: New data to constrain the Mesoamerica secular variation curve

Seminar plan

- Why is the topic interesting?
- What were the major assumptions?
- What were the major findings?
- What would the next steps be?

- Why is this paper interesting?
  - archeomagnetic studies provide constraints for global field models (e.g., CALSK and ARCH types of models)
  - once we have a good model, archeologists can use magnetic vectors to constrain ages on artifacts
- North America (including Mexico) has very few good data - so Mexico is a high priority for archeomagnetic research in general

Field models 101

Why study the magnetic field at all?

- Acts as shield for solar and cosmic radiation
- controls production of cosmogenic nuclides (^{14}C, ^{10}Be....)
- may play a role in nucleating clouds...
- navigation
- is a window into processes into the deep earth

How can we study it?

- Numerical simulation
- Direct observations (satellites, geomagnetic observatories, and other human measurements)
- Indirect records (archaeological and geological materials)

How the data are used:

A magnetic field (H) is the gradient of a magnetic potential:

$$\mathbf{H} = -\nabla \psi_m$$

simplest case: $\psi_m = \dfrac{\mathbf{m} \cdot \mathbf{r}}{4\pi r^3} = \dfrac{m \cos\theta}{4\pi r^2}$

So, knowing m, we can evaluate H anywhere and vice versa

$$H_r = -\frac{\partial \psi_m}{\partial r} = \frac{1}{4\pi} \frac{2m \cos\theta}{r^3}$$

$$H_\theta = -\frac{1}{r} \frac{\partial \psi_m}{\partial \theta} = \frac{m \sin\theta}{4\pi r^3}$$

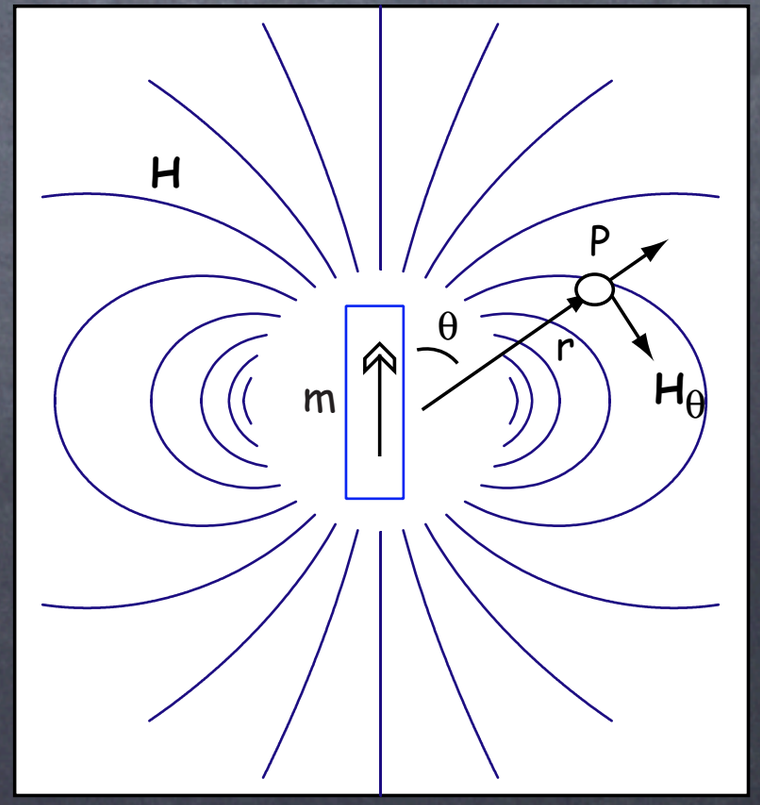

Elements of the magnetic field

Not a perfect dipole

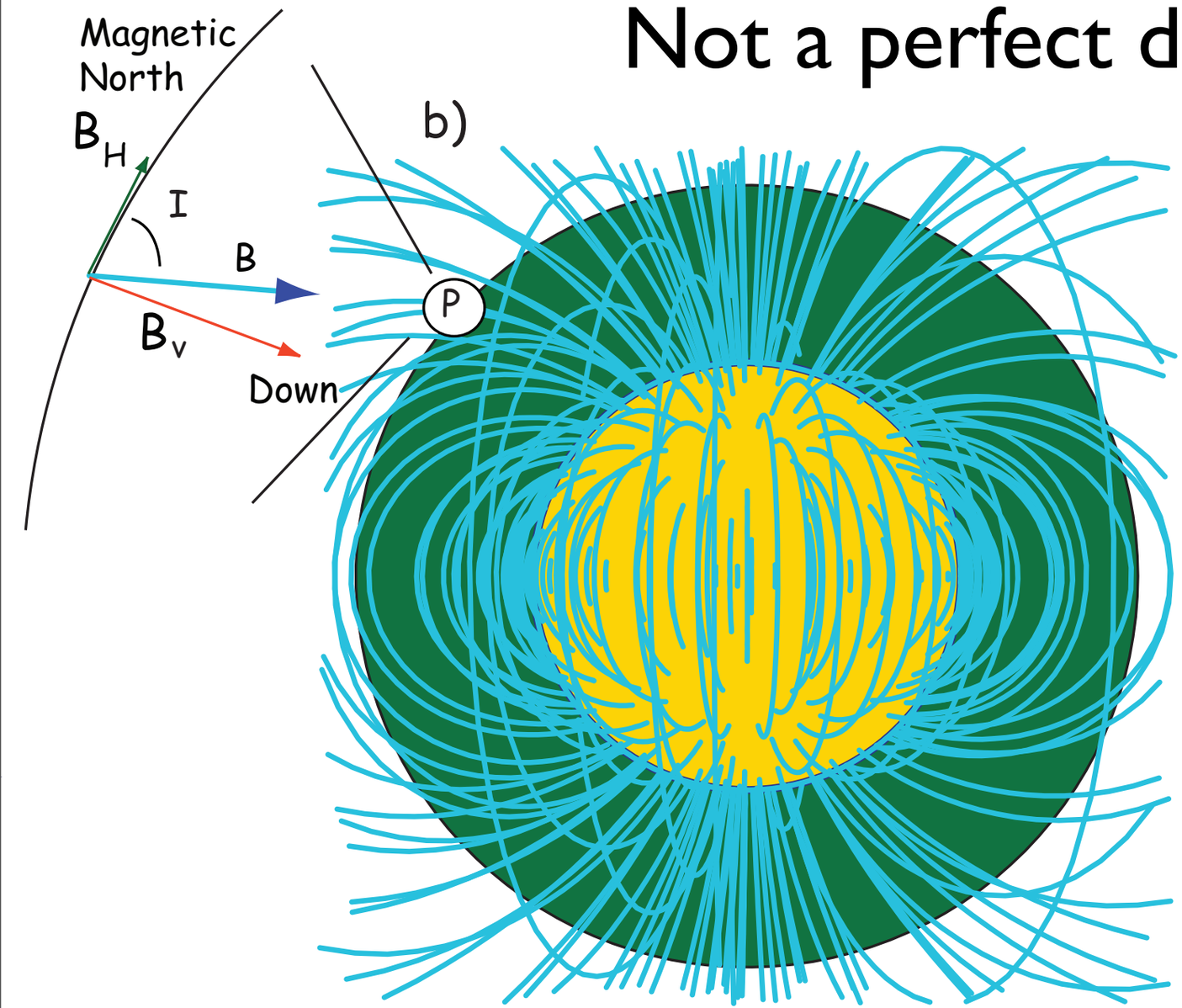

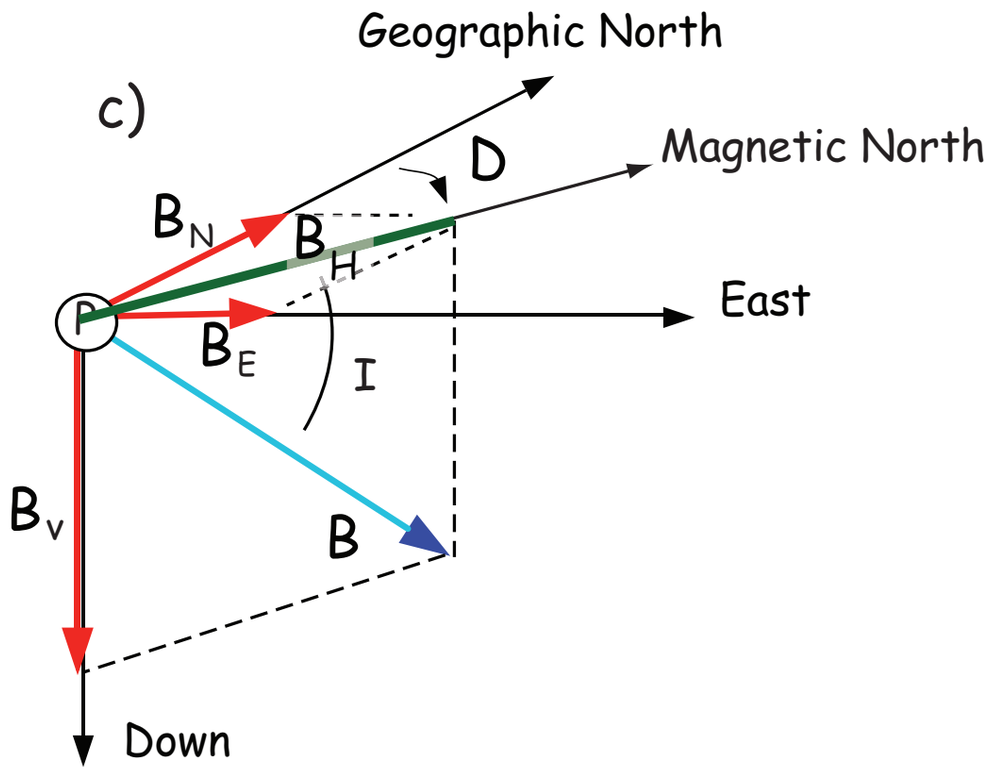

Geomagnetic potential:

$$\psi_m(r,\theta,\phi) = \frac{a}{\mu_o}\sum_{l=1}^{\infty}\sum_{m=0}^{l}\left(\frac{a}{r}\right)^{l+1} P_l^m(\cos\theta)\,(g_l^m\cos m\phi + h_l^m \sin m\phi)$$

So, we need a whole list of numbers g_l^m and h_l^m

(International Geomagnetic Reference Fields - IGRF)

These are best-fits from the observations for a given year.

These lists allow us to predict the geomagnetic field vector at any point outside the core

- so data from archeomagnetic studies can get plugged directly into constraining IGRF-like models.

Why Mexico?: Analysis of ArcheoInt database (Genevey et al., 2008 - http://earthref.org/ERDA/887/) shows that Mexico has very few datapoints.

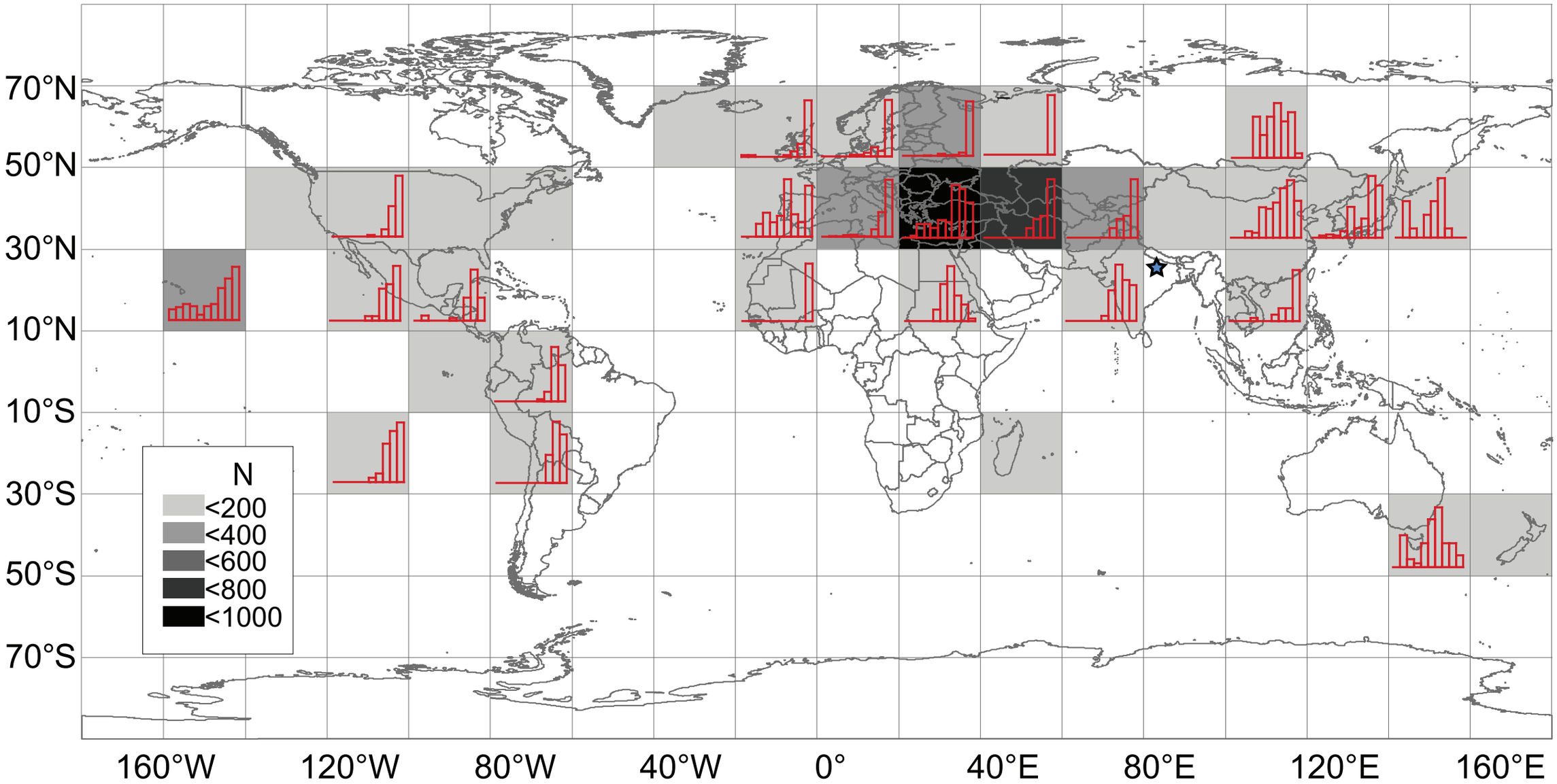

Figure from Mitra et al., 2013, (http://dx.doi.org/10.1016/j.epsl.2012.12.027) supplemental material

Which brings us to "This week in Pmag:"

Earth and Planetary Science Letters 363 (2013) 168–180

Contents lists available at SciVerse ScienceDirect

Earth and Planetary Science Letters

journal homepage: www.elsevier.com/locate/epsl

First archeointensity determinations on Maya incense burners from Palenque temples, Mexico: New data to constrain the Mesoamerica secular variation curve

G. Fanjat [a], P. Camps [a,*], L.M. Alva Valdivia [b], M.T. Sougrati [d], M. Cuevas-Garcia [c], M. Perrin [e]

[a] Géosciences Montpellier, CNRS and Université de Montpellier 2, Montpellier, France
[b] Laboratorio de Paleomagnetismo, Instituto de Geofísica, Universidad Nacional Autonoma de Mexico, México D.F., Mexico
[c] Instituto Nacional de Antropologia e Historia, México D.F., Mexico
[d] Institut Charles Gerhardt, Laboratoire des Agrégats, Interfaces et Matériaux pour l'Energie, 34095 Montpellier, France
[e] Aix-Marseille Université, CNRS, IRD, CEREGE UM34, 13545 Aix en Provence, France

Major assumptions

- Mayan incense burners can be dated to within +/- 50 years
- Thellier-Thellier method (with corrections) yields an accurate paleointensity estimate

Outline of the paper

- Location, age and description of samples
- sample characterization
- Archeointensity experiment
- Results/Conclusions

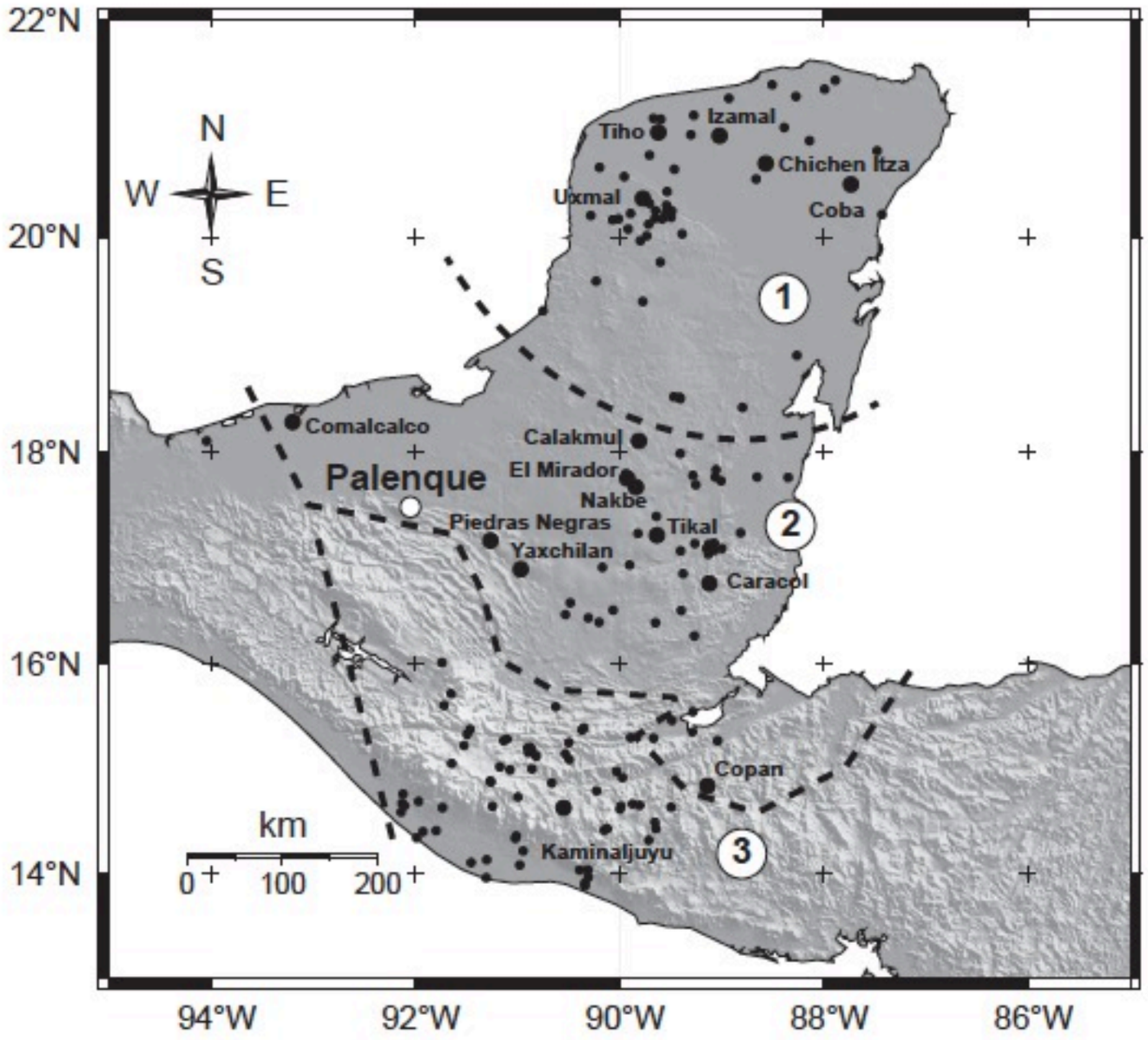

Fig. 1. Map of the Maya region showing locations of some of the principal cities (filled circles). Bigger symbols and labels are plotted for the most important cities. The thick dashed lines delimit the northern lowlands (1), the central lowlands (2), and the highlands and Pacific coast (3) cities.

Fanjat et al., (2013)

Fig. 2. Two incense burner pedestals from (a) Temple of the Foliated Cross (TCF-13/93, Balunté ceramic phase) and (b) Temple of the Cross (TC-5/93, Otulum ceramic phase), from Cuevas-García (2007).

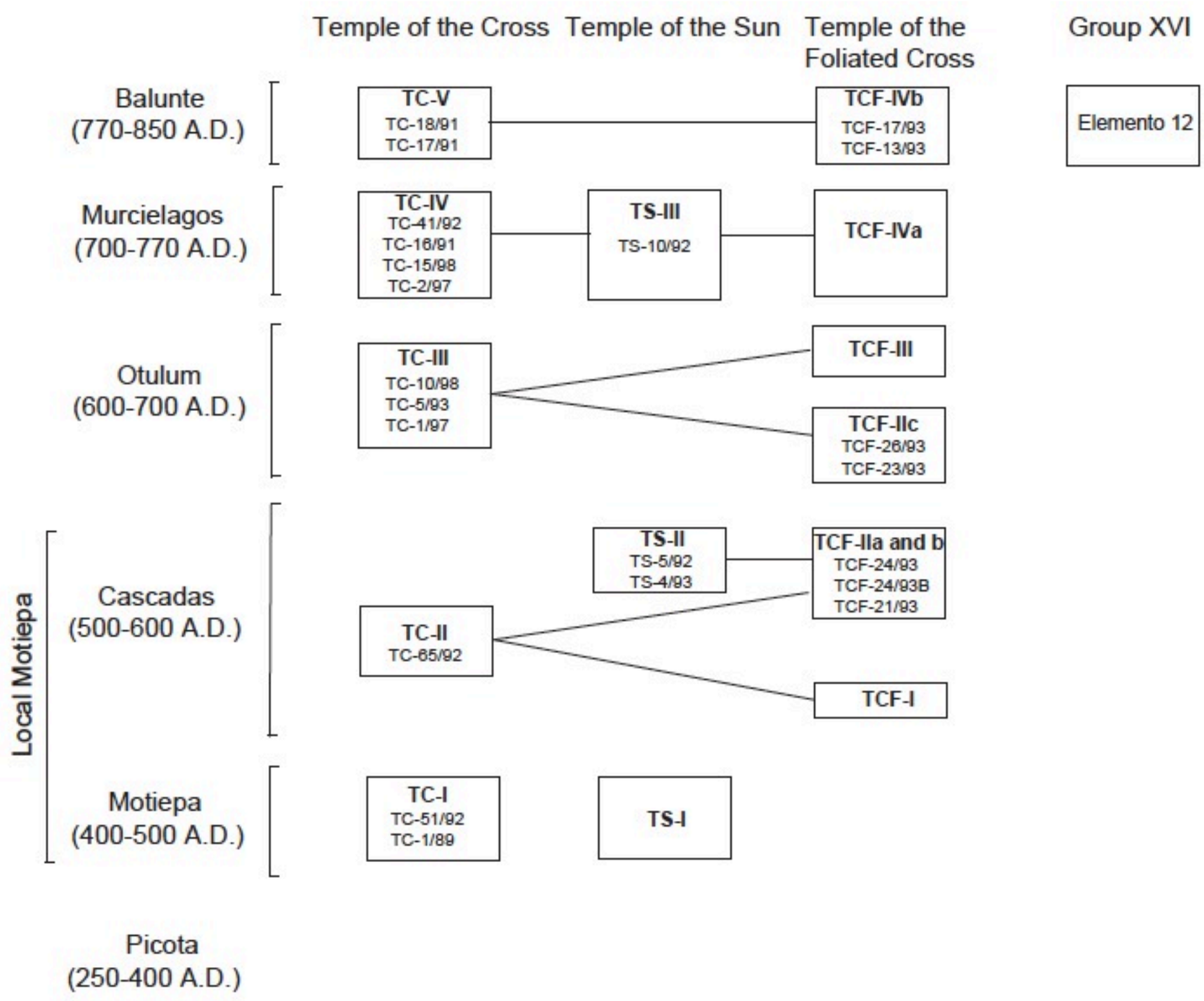

Fig. 3. Schematic classification of the incense burners of the group of temples of the cross (redrawn from Cuevas-García, 2007; Rands, 2007).

Fanjat et al., (2013)

Sample characterization

- K-T curves
- Hysteresis loops
- X-ray powder diffraction
- Moessbauer

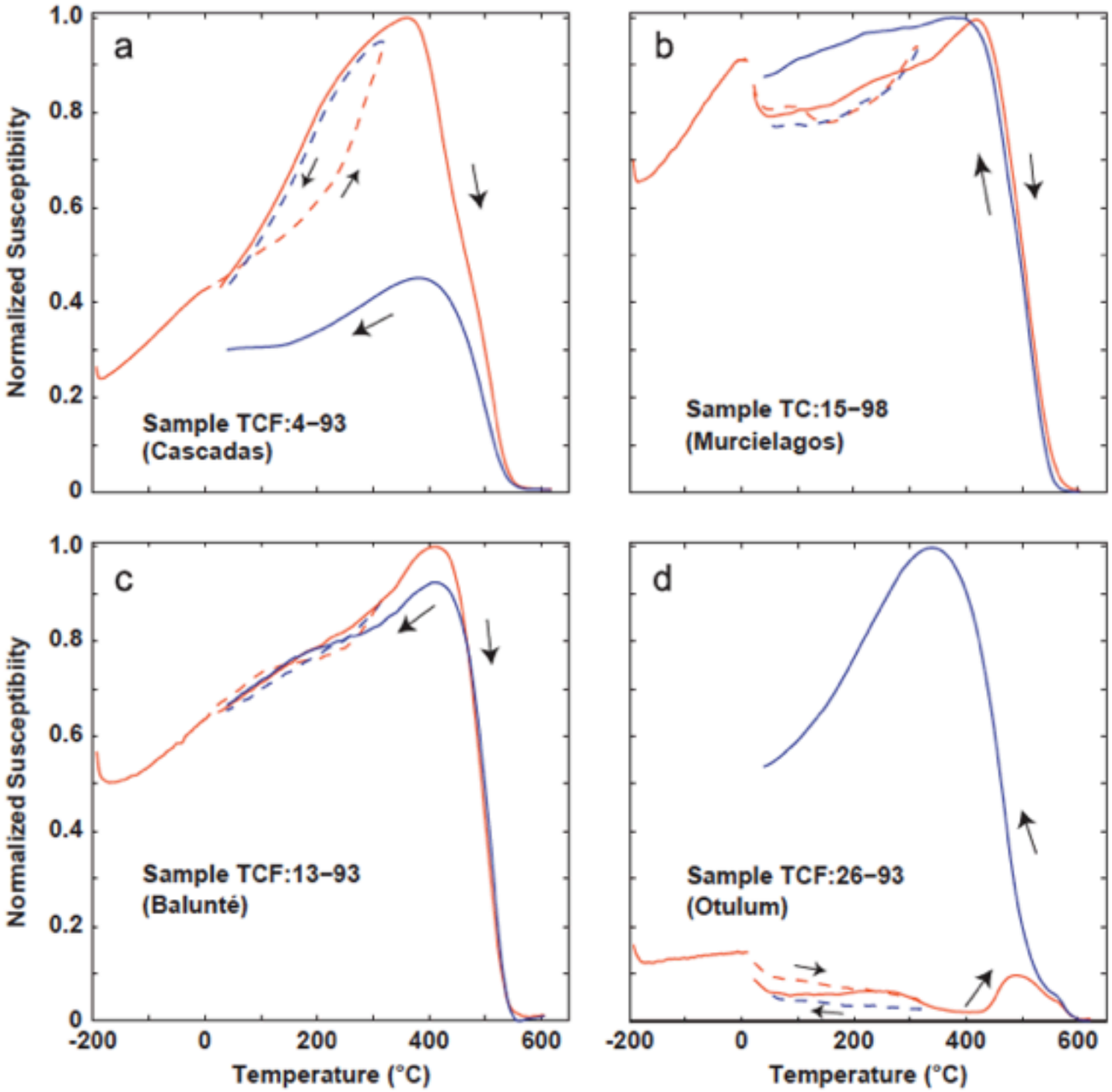

Fig. 4. Representative examples of low-field susceptibility versus temperature curves measured under air atmosphere (*K–T* curves). Susceptibility values are normalized to the maximum susceptibility. The heating curves are in red, the cooling curves are in blue. The dashed lines correspond to partial heating–cooling cycles. (For interpretation of the references to color in this figure legend, the reader is referred to the web version of this article.)

Hysteresis ratios:

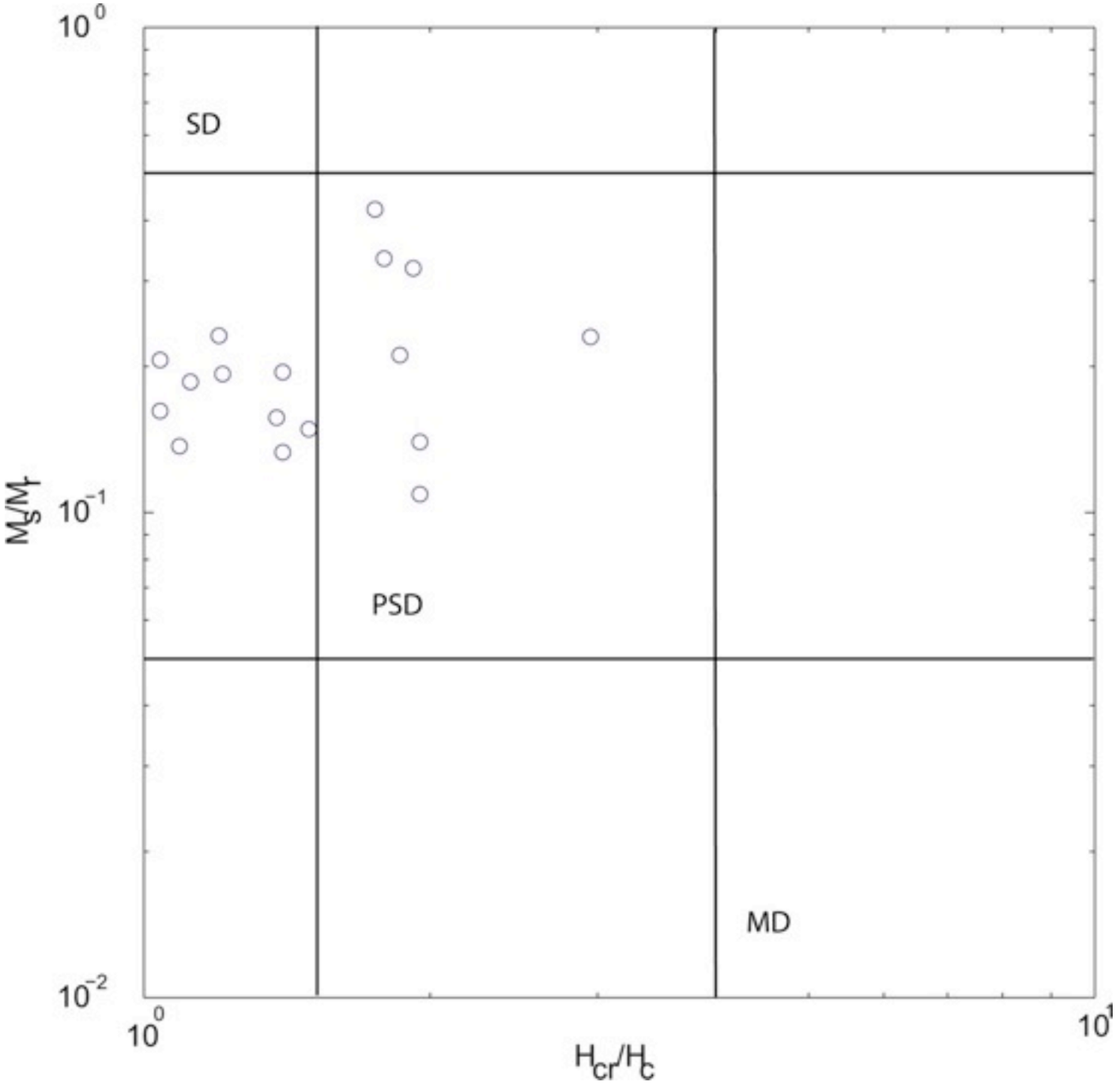

Questions:
1) what do these ratios mean without seeing the actual loops?
2) do these help in anyway in selecting 'reliable' data?

Fanjat et al., (2013) - Figure S1

X-ray Powder Diffraction: says "The absence of primary clay minerals such as illite, smectite or calcite or few remains of muscovite and the presence of high-T new phases such as K-feldspar or anorthite are arguments in favor of a firing temperature minimum to 700°C."

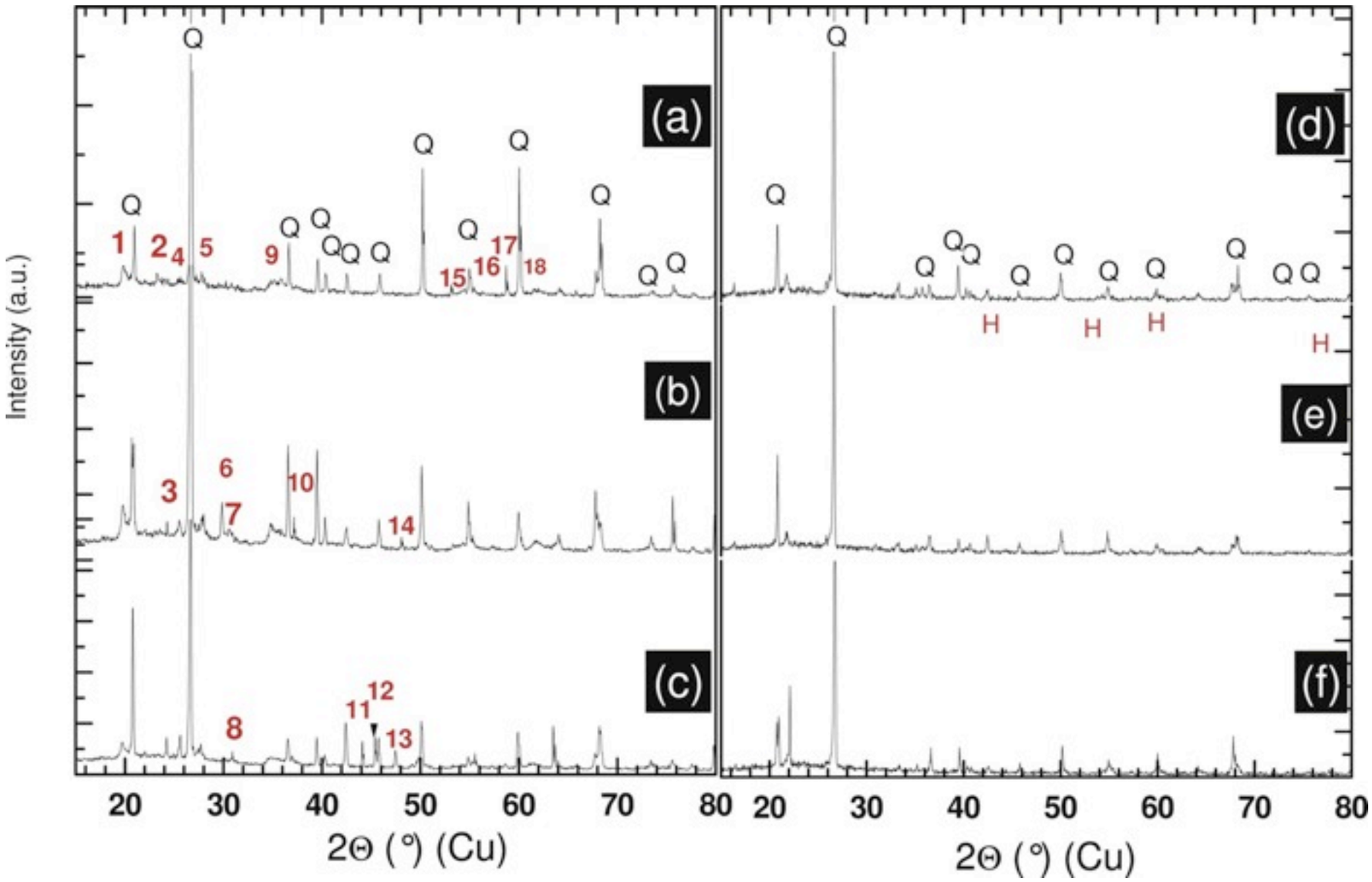

Fanjat et al. (2013) - Supplemental Figure S2

Moessbauer says: firing temperatures >400-850C

before

after

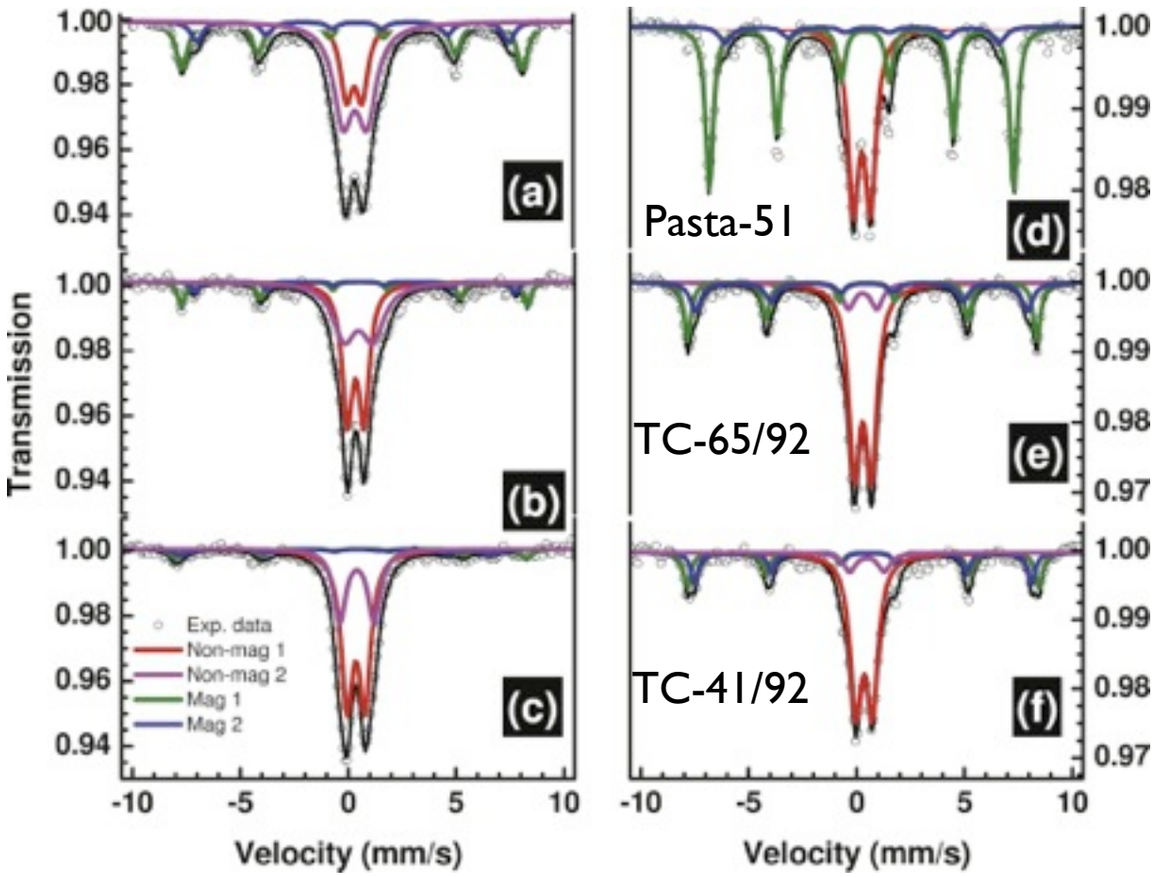

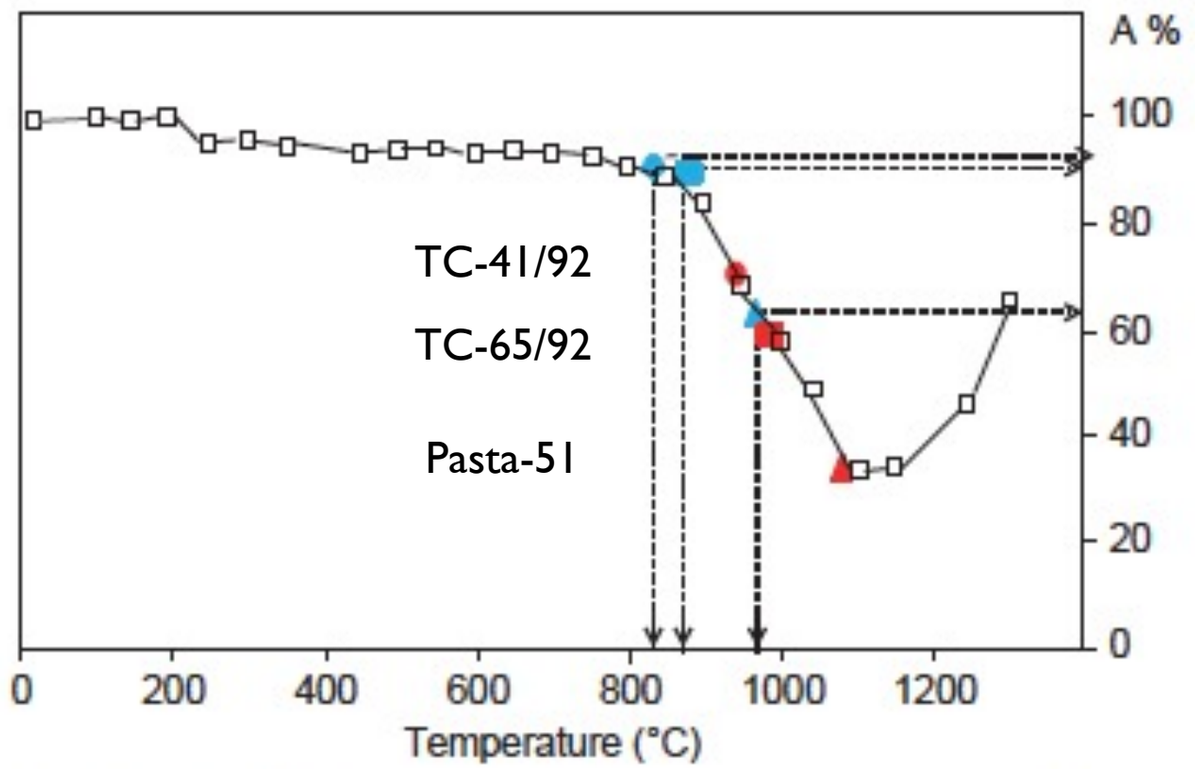

Fig. 5. Estimated firing temperature based on the non-magnetic iron (right axis). Figure adapted from Murad and Wagner (1989). Pasta 51: triangle, TC-65/92: squares and TC-41/92: circles. Blue (red) symbols are measurements before (after) laboratory firing. (For interpretation of the references to color in this figure legend, the reader is referred to the web version of this article.)

Fanjat et al. (2013) - Supplemental Figure S3

(a lot of assumptions went into this interpretation)

Archeointensity experiment

- Thellier-Thellier experiment (in-field/in-field) - imported supplemental datafile into MagIC
- Anisotropy correction - used a low temperature (290C) ATRM correction
- Cooling rate correction: empirical slow versus fast cooling comparison

1. Archeointensity measurements are represented with Arai's diagram in which the NRM left is plotted against the pTRM acquired after each heating step. The slope of the least-squares-fit line computed from the linear part of the diagram gives an estimate of the archeointensity. A value is accepted when the linear segment is defined by more than four points ($n > 4$) and spans over 30% of the total extrapolated ChRM ($f > 0.3$).
2. pTRM checks estimate the thermal alteration of magnetic properties for each sample and assess the reliability of the archeointensity. We quantified the difference between two pTRM acquisitions at the same temperature step with the Difference Ratio (DRAT) parameter (Selkin and Tauxe, 2000). DRAT corresponds to the maximum difference measured in percent between two repeated pTRM acquisition normalized by the length of the selected NRM-TRM segment. We fixed arbitrarily a maximum acceptable DRAT of 10%.
3. Finally, we checked on the Zijderveld plots computed from the archeointensity measurements that the NRM fraction used to calculate the archeointensity may correspond to the ChRM, or at least to a part of the whole ChRM. The low-temperature part of the NRM may contain natural secondary magnetizations, and at high temperature a chemical remanent magnetization may be acquired during the laboratory heating. This check is performed qualitatively by a visual inspection of the vector endpoint diagrams. The points in the selected interval should trend toward the origin if the NRM is the ChRM.

“low firing temperature”

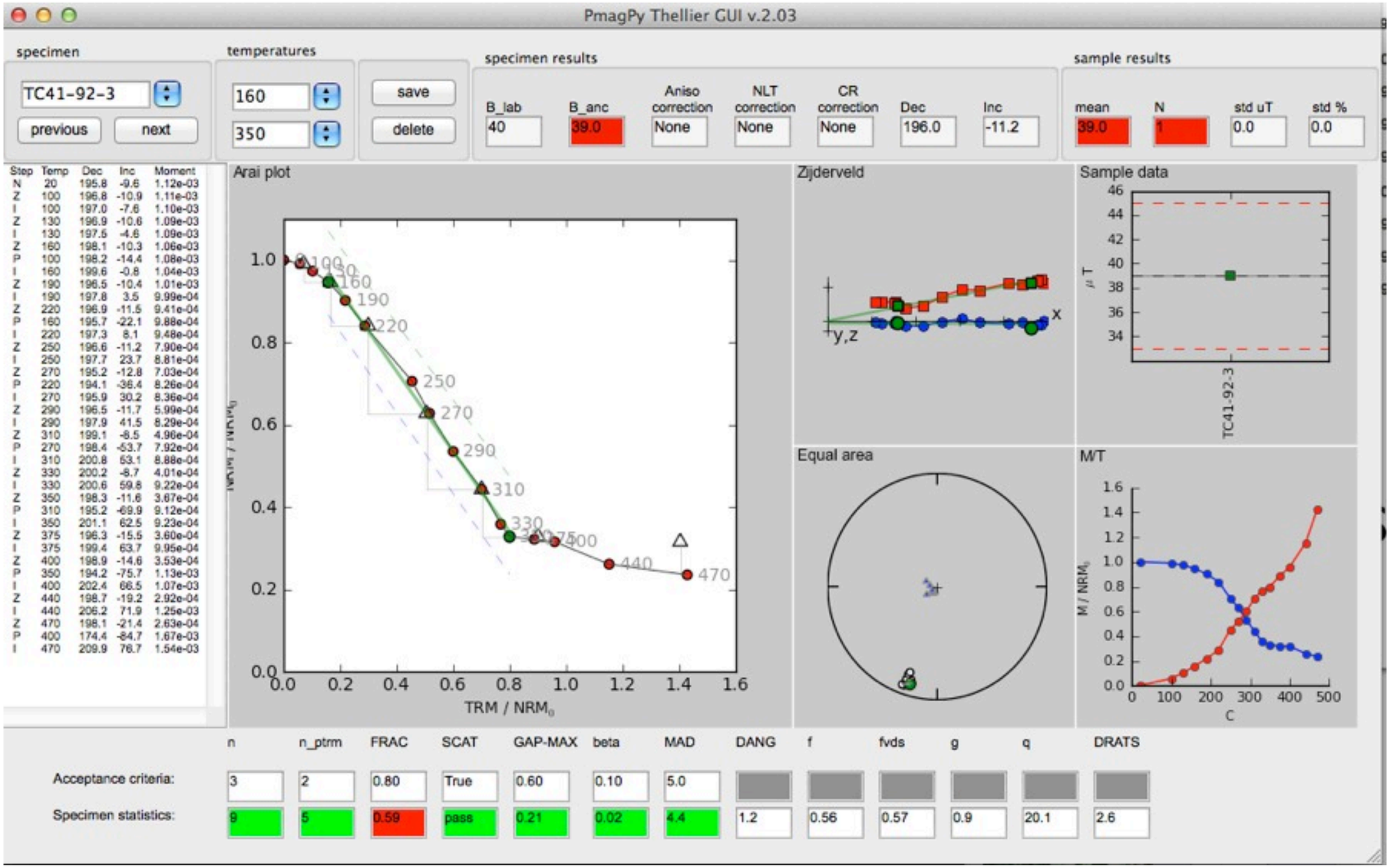

Fanjat et al. (2013) supplemental data, imported to MagIC format and rendered with thellier_gui.py of Shaar and Tauxe (2013)

medium firing temperatures

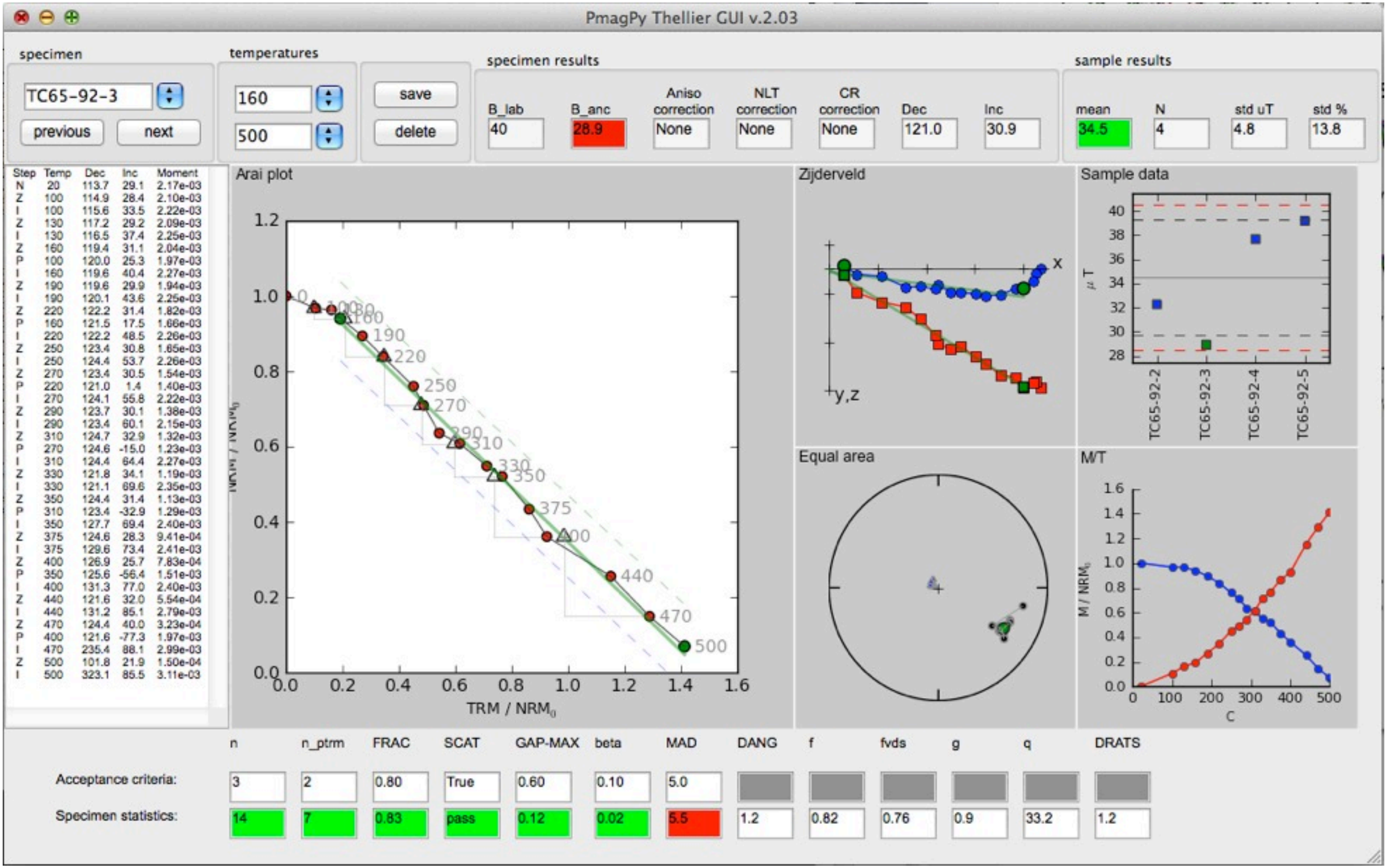

Fanjat et al. (2013) supplemental data, imported to MagIC format and rendered with thellier_gui.py of Shaar and Tauxe (2013)

high firing temperature

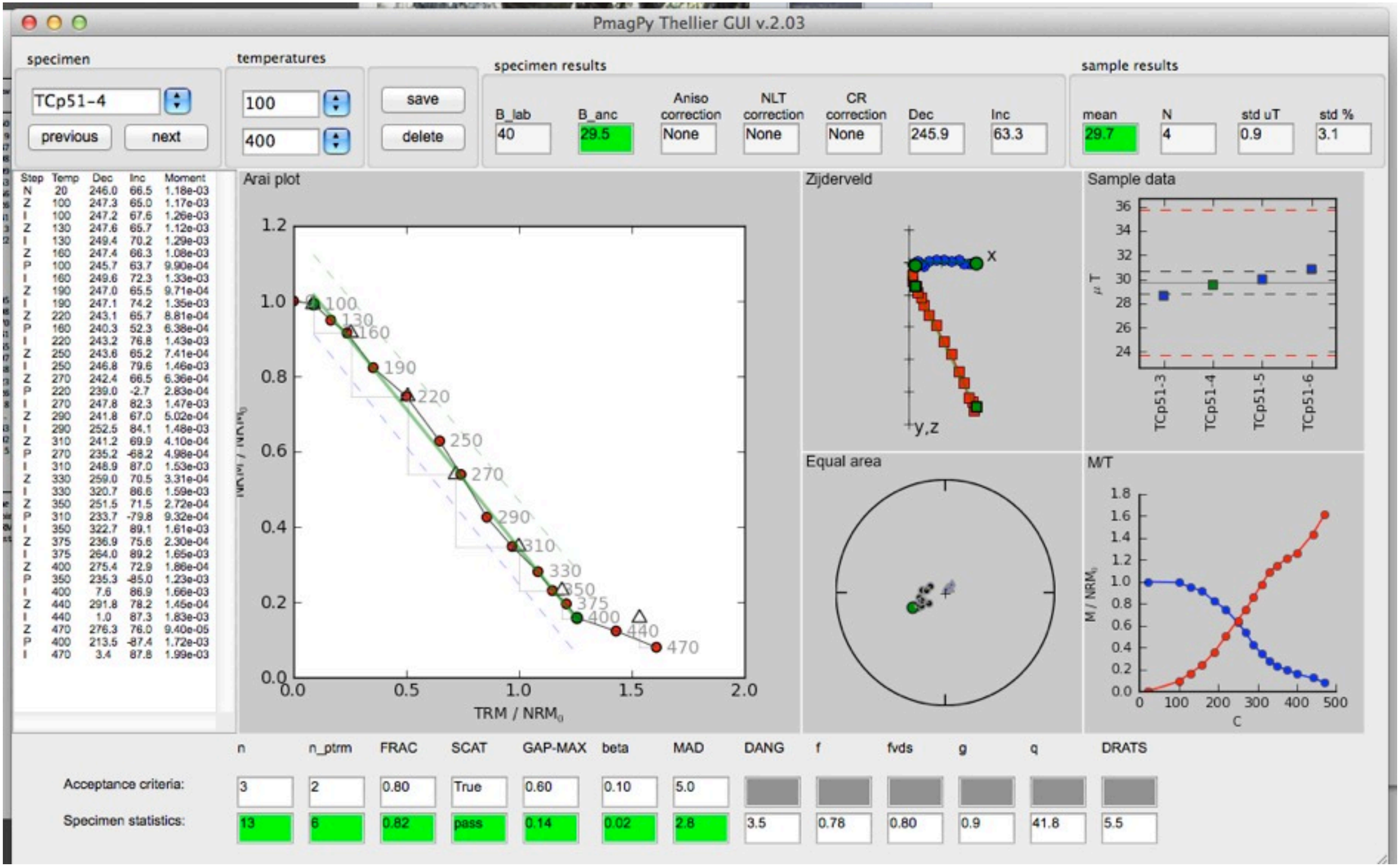

Fanjat et al. (2013) supplemental data, imported to MagIC format and rendered with thellier_gui.py of Shaar and Tauxe (2013)

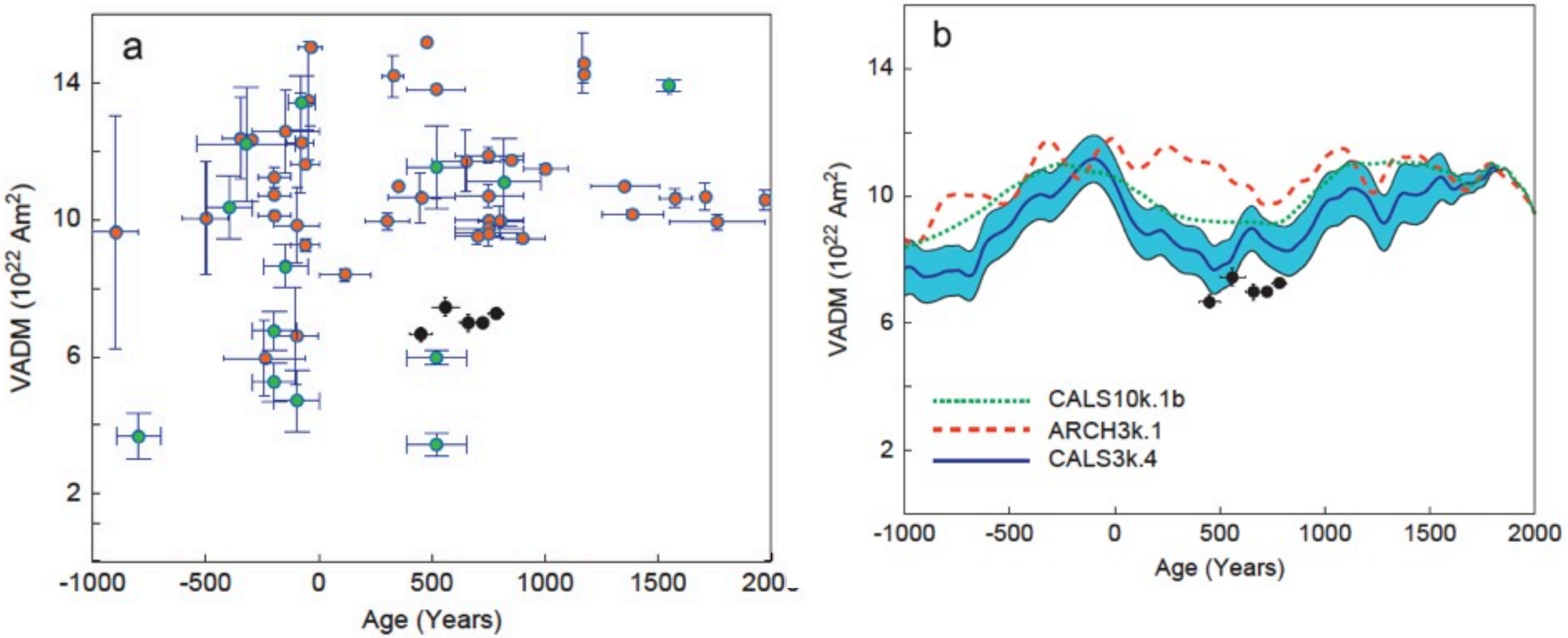

Fig. 7. Compilation of archeointensity VADM data selected for Mesoamerica as explained in the text and Fig. 6. (a) All selected data of good (poor) technical quality are plotted in green (red) altogether with the present study data (black circles). (b) Confrontation of our Palenque VADM with the CALS3k.4 global model (blue line) represented with its 95% confidence interval (shaded area). The models CALS10k.1b (green dotted line) and ARCH3.1 (red dashed line) are also represented. (For interpretation of the references to color in this figure legend, the reader is referred to the web version of this article.)

Major findings

- Previously published data are highly scattered and lack experimental credibility.
- New results are not compatible with any of the models.
- Not much variability - ranges from 67-74 ZAm^2
- Results could be used to refine chronology of the Motiepa phase

Next steps

- Need more data
- what about a different way of doing firing temperature (Bernasconi et al., 2011)

Available online at www.sciencedirect.com

ScienceDirect

Journal of the European Ceramic Society 31 (2011) 1353–1360

www.elsevier.com/locate/jeurceramsoc

The role of firing temperature, firing time and quartz grain size on phase-formation, thermal dilatation and water absorption in sanitary-ware vitreous bodies

A. Bernasconi [a], V. Diella [b,*], A. Pagani [b], A. Pavese [a,b], F. Francescon [c], K. Young [d], J. Stuart [d], L. Tunnicliffe [d]

[a] *Dipartimento di Scienze della Terra, Università di Milano, Via Botticelli 23, I-20133 Milano, Italy*
[b] *National Research Council, IDPA, Section of Milan, Via Botticelli 23, I-20133 Milano, Italy*
[c] *Ideal Standard International, C.O.E., Ceramic Process Technology, Via Cavassico Inferiore 160, I-32026 Trichiana (BL), Italy*
[d] *SIBELCO, Group Central Laboratory, Moneystone Quarry, Whiston, Stoke-on-Trent ST10 2DZ, United Kingdom*

Received 18 November 2010; received in revised form 21 January 2011; accepted 3 February 2011

Abstract

This work reports a study on (i) the evolution of mineral phases versus time and temperature, and (ii) some relationships between phases observed, process parameters, and macroscopic properties (thermal expansion and water absorption), in sanitary-ware vitreous bodies. These properties are relevant to satisfying the technical requirements of sanitary-ware. We have fixed the green body composition, varying some key process parameters, such as firing temperature (T_f), firing time (t_f) and quartz grain size (d_{50}); a grid of 30 T_f–t_f–d_{50} points has been explored. We have spanned the t_f–T_f space (0–80 min; 1200–1280 °C) using firing temperatures representative of the plateau values of the heating curve in industrial processes. X-ray powder diffraction has been used to determine the phase composition for each T_f–t_f–d_{50} point. Scanning electron microscopy proved useful in enhancing the micro-structural characterization. Quartz d_{50} seems to be the process-parameter which most effectively co-relates with the thermal expansion of the glassy matrix.

Keywords: Firing; Traditional ceramics; X-ray methods; Water absorption; Thermal expansion